

Unsaturated Single Atoms on Monolayer Transition Metal Dichalcogenides for Ultrafast Hydrogen Evolution

Yuting Luo^{1†}, Shuqing Zhang^{1†}, Haiyang Pan², Shujie Xiao³, Zenglong Guo⁴, Lei Tang¹, Usman Khan¹, Baofu Ding¹, Meng Li⁵, Zhengyang Cai¹, Yue Zhao², Wei Lv³, Qinliang Feng⁵, Xiaolong Zou^{1*}, Junhao Lin^{4*}, Hui-Ming Cheng^{1,6}, & Bilu Liu^{1*}

¹ Shenzhen Geim Graphene Center (SGC), Tsinghua-Berkeley Shenzhen Institute (TBSI), Tsinghua University, Shenzhen 518055, P. R. China.

² Institute for Quantum Science and Engineering, Southern University of Science and Technology, Shenzhen 518055, P. R. China.

³ Graduate School at Shenzhen, Tsinghua University, Shenzhen 518055, P. R. China.

⁴ Department of Physics, Southern University of Science and Technology, Shenzhen 518055, P. R. China.

⁵ MOE Key Laboratory of Material Physics and Chemistry under Extraordinary Conditions, Shaanxi Key Laboratory of Optical Information Technology, School of Science, Northwestern Polytechnical University, Xi'an 710072, P. R. China.

⁶ Shenyang National Laboratory for Materials Science, Institute of Metal Research, Chinese Academy of Sciences, Shenyang 110016, P. R. China.

† These authors contribute equally.

Correspondence should be addressed to B.L. (email: bilu.liu@sz.tsinghua.edu.cn), J.L. (email: linjh@sustech.edu.cn), or X.Z. (email: xlzou@sz.tsinghua.edu.cn).

SUMMARY

Large scale implementation of electrochemical water splitting for hydrogen evolution requires cheap and efficient catalysts to replace expensive platinum. Molybdenum disulfide is one of the most promising alternative catalysts but its intrinsic activity is still inferior to platinum. There is therefore a need to explore new active site origins in molybdenum disulfide with ultrafast reaction kinetics and to understand their mechanisms. Here, we report a universal cold hydrogen plasma reduction method for synthesizing different single atoms sitting on two-dimensional monolayers. In case of molybdenum disulfide, we design and identify a new type of active site, *i.e.*, unsaturated Mo single atoms on cogenetic monolayer molybdenum disulfide. The catalyst shows exceptional intrinsic activity with a Tafel slope of 35.1 mV dec⁻¹ and a turnover frequency of $\sim 10^3$ s⁻¹ at 100 mV, based on single flake microcell measurements. Theoretical studies indicate that coordinately unsaturated Mo single atoms sitting on molybdenum disulfide increase the bond strength between adsorbed hydrogen atoms and the substrates through hybridization, leading to fast hydrogen adsorption/desorption kinetics and superior hydrogen evolution activity. This work shines fresh light on preparing highly-efficient electrocatalysts for water splitting and other electrochemical processes, as well as provides a general method to synthesize single atoms on two-dimensional monolayers.

INTRODUCTION

Concerns about the energy crisis and environmental pollution have called for the development of hydrogen, a clean and high density energy carrier, as a key alternative to fossil fuels.^{1,2} Currently, hydrogen has been mainly produced using carbon-based resources, *i.e.*, natural gas, oil, and coal,

making carbon emission unavoidable.³ The production of hydrogen by electrochemical water splitting promises to overcome this challenge, especially when the reaction is driven by electricity generated by renewable energy such as solar and wind. However, the hydrogen evolution reaction (HER) has a much lower thermal efficiency than its thermodynamic limit, resulting in the need of using highly efficient electrocatalysts. Platinum (Pt) has been proved to be the most efficient HER catalyst, but its scarcity and high cost hamper its wide use. In recent years, various Pt-free materials have been explored as alternative HER electrocatalysts, including metal alloys,^{4,5} metal hydroxides,^{6,7} metal disulfides,⁸⁻¹⁰ metal carbides,^{11,12} and metal phosphides^{13,14}. Nevertheless, the intrinsic HER activities of these catalysts are still inferior to Pt. Increasing the numbers of active sites may endow catalysts with decent HER performance, but also make the mechanism study difficult. Noteworthy, monolayer two-dimensional (2D) materials possess unambiguous crystal structures and accurately determined reaction area¹⁵⁻¹⁷, *i.e.*, nearly identical interface area and electrode area, serving as ideal models to investigate intrinsic activity of catalysts (**Figure. S1**). Among various 2D materials, molybdenum disulfide (MoS₂) is promising due to its earth abundance and good stability.¹⁸ Interest in MoS₂ catalyst can be traced back to the 1970s in the hydrodesulphurization (HDS) processes, where it was used to remove sulfur and add hydrogen in hydrocarbon streams.^{19,20} As HER shares a similar H* intermediate with the HDS reaction, MoS₂ was also found to be active for the HER in 2007, where the edges of 2D MoS₂ were found to be the active sites.^{21,22} Later, it was shown that phase transformation of MoS₂ from the stable 2H phase to the metastable 1T phase activates the inert basal plane of MoS₂ for the HER.^{23,24} The sulfur vacancies (S vacancies) and strain in MoS₂ were later found to be active for the HER.^{25,26} After that, researchers have devoted much effort to synthesize 2D MoS₂ for better HER activity by creating more active sites including edges, the 1T phase, S vacancies, or strain (**Figure**

1A).²⁷⁻³¹ However, the HER activities of 2D MoS₂ (usually with overpotentials larger than 170 mV at 10 mA cm⁻² and Tafel slopes larger than 40 mV dec⁻¹) are still inferior to Pt-based catalysts (**Table S1**).^{15,30,32-35} This calls for the search for new active sites in MoS₂ to further improve its HER performance.

On the other side, single atoms (SAs) have become important in recent years, because they show great potential as highly efficient catalysts with a higher catalytic activity per atom site and better stability than nanoparticle catalysts.³⁶ SAs have the simplest structures usually with only one atom as the active site, and thus in principle, could be ideal for studying the mechanism of catalytic process. For example, multinuclear active sites are commonly necessary for water oxidation, while recently Guan *et al.*³⁷ reported that Mn SAs embedded in nitrogen-doped graphene is effective in the oxygen evolution reaction, suggesting that a mononuclear active site is capable for oxygen evolution. Note that although SAs have well-defined structures, they are usually loaded on bulk or multilayer supports with different structures, making their microscopic chemical environment, coordination conditions, and structures complicated. Ideally, one can use supports with clear and well-defined structures such as 2D monolayers to support SAs. On one hand, this will simplify the system which in turn benefits the mechanism study. This is because monolayer supports are suitable for obtaining better statistical density of SAs, not only the mass density (wt%) and atom density (at%) widely used for SAs on porous or bulk supports in literature, but also the area density (atom nm⁻²) and volume density (atom nm⁻³) which are only accurate in atomically thin 2D supports. On the other hand, for cases like 2D MoS₂, combining SAs with monolayer MoS₂ may bring opportunities to create new types of active sites to further improve its HER activity. Unfortunately, the synthesis of metal SAs on 2D monolayer supports is still a grand challenge and has rarely been reported.

Here, we develop a cold hydrogen plasma reduction method and successfully synthesize different SAs/2D monolayer systems, where SAs sit on 2D monolayers. Our idea is inspired by the fact that hydrogen plasma shows a strong reducibility and in principle can dissociate chemical bonds between anions and metal cations in metal compounds.³⁸⁻⁴⁰ For an exemplified system of Mo SAs sitting on cogenetic MoS₂ monolayers (denoted as Mo SAs/ML-MoS₂), experimental and theoretical results show that the Mo SAs are coordinately unsaturated since Mo SAs transfer less charge to sulfur atoms than do saturated Mo atoms in the pristine MoS₂. We use this Mo SAs/ML-MoS₂ system as a HER model catalyst (**Figure 1B**) based on the following considerations. First, it is assumed that the active sites on MoS₂ for HDS are unsaturated Mo centers,¹⁸ showing certain similarity to HER activity given by unsaturated Mo atoms near S vacancies.²⁴ We therefore expect unsaturated Mo SAs to have a decent HER activity. Second, a Mo SA on monolayer MoS₂ has a simple and well-defined structure, which is suitable for the study of its HER kinetics and understanding the mechanism. Electrochemical measurements based on single MoS₂ flake microcells show that Mo SAs/ML-MoS₂ catalysts show ultrafast HER kinetics with a small Tafel slope of 35.1 mV dce⁻¹ and an impressively high turnover frequency (TOF) of $\sim 10^3$ s⁻¹ at 100 mV. By the analyses of the density of states, we find that an unsaturated Mo SA on MoS₂ effectively hybridizes with H, leading to increased H bonding and a lower Fermi level for the hydrogen adsorption compared to saturated Mo systems. An almost zero hydrogen adsorption free energy is achieved in Mo SAs/ML-MoS₂, giving rise to the superior intrinsic activity for the HER.

RESULTS

As shown in **Figure 1C**, we developed a new and universal strategy for treating 2D monolayers by a

cold hydrogen plasma to obtain metal SAs on 2D monolayers. In principle, when conditions are controlled properly, the hydrogen plasma which has a stronger reducing ability than hydrogen molecules,^{38,39} may bond with anions like sulfur atoms and dissociate metal atoms at a low temperature, generating metal SAs on 2D monolayers. Take Mo SAs/ML-MoS₂ system as an example, where Mo SAs sitting on the monolayer MoS₂ (**Figure 1B**). The Mo SAs/ML-MoS₂ system was synthesized by a two-step method (see details in the “**Methods**” section and **Figure S2**). First, ML-MoS₂ was grown on a SiO₂/Si substrate by chemical vapor deposition (CVD) at a growth temperature of 750 °C. The monolayer nature of the MoS₂ was demonstrated by atomic force microscopy (AFM), photoluminescence (PL), and Raman spectroscopy (**Figure S3**). Second, the sample was treated by the hydrogen plasma under different conditions. Besides MoS₂, we prepared W SAs on monolayer WS₂ (denoted as W SAs/ML-WS₂, **Figure 1D**) by this method (see details in **Supplemental Information**). We studied several parameters in the plasma process including temperature, pressure, time and radio frequency power, and found that temperature especially played a key role. When the temperature is above 200 °C, dissociation of the Mo-S bonds becomes easy and large holes appear in the monolayer MoS₂ (**Figure S4**), consistent with a previous report.⁴¹ Therefore, we control the temperature to be below 80 °C, which is monitored by a thermocouple in the plasma chamber, to avoid destruction of the structure of the MoS₂ flakes and aggregation of Mo atoms. Under proper conditions, no obvious structural changes like holes or cracks appear in the Mo SAs/ML-MoS₂ samples (**Figure S5**). The best sample was prepared with a H₂ flow rate of 20 standard cubic centimeters per minute (sccm) and a radio frequency power smaller than 30 W for 80 s, which contained abundant Mo SAs on monolayer MoS₂. The key to synthesize Mo SAs/ML-MoS₂ is to control the reaction by kinetics rather than thermodynamics. MoS₂ flakes prepared by the Scotch tape exfoliation method behaved the same as

the CVD-grown MoS₂ upon hydrogen plasma treatment (**Figure S6**). We also examined the use of an Ar plasma instead of the hydrogen plasma (under similar pressure, time, power of radio frequency, and temperature), and found that the degree of reduction of the Mo decreases, showing that hydrogen is necessary because of its strong reducing ability being able to chemically dissociate the Mo-S bonds in MoS₂ (**Figure S7**).

To study the microscopic structure of the SAs/2D monolayer samples, high-angle annular dark-field STEM (HAADF-STEM) characterization was performed on both pristine MoS₂ and Mo SAs/ML-MoS₂ samples for comparison. As shown in **Figure S8A**, the pristine MoS₂ shows a hexagonal crystal structure with alternating bright and dark spots, which are assigned to columns of Mo and S₂ according to their atomic weight. We occasionally observe a few sites whose intensity is higher than that of their neighbors (**Figure S8A**). Combined with energy dispersive spectroscopy (EDS), X-ray photoelectron spectroscopy (XPS), and image simulation (**Figures. S9-S11**), these brighter sites are recognized as Mo SAs. Similar results were also reported by Hong *et al*, suggesting that trace amount of Mo adatoms present in CVD-grown MoS₂ samples.⁴² The density of Mo SAs in the pristine MoS₂ was measured to be 0.0051 atoms nm⁻², while after hydrogen plasma treatment the HAADF-STEM images of Mo SAs/ML-MoS₂ sample show that the density of Mo SAs has increased to 0.4365 atoms nm⁻², almost two orders of magnitude higher than that of the pristine MoS₂ sample (**Figure 1D, Figures. S8B and S8C**). The Mo SAs/ML-MoS₂ sample shows SA densities that are similar to recent reports, having a mass density of 2.21 wt% and an atom density of 1.23 at% (**Table S2**). Moreover, thanks to the clear crystal structure of the ML-MoS₂ support, we estimated the area density of Mo SAs on Mo SAs/ML-MoS₂ to be 4.35×10^{13} atoms cm⁻², which cannot be estimated in the case of porous or bulk supports.

We also found that the Mo SAs/ML-MoS₂ samples retain the well-defined hexagonal lattice without noticeable damage to the basal planes of the original lattice. To further verify the integrity of the MoS₂ lattice, we compared the densities of S vacancies for pristine MoS₂ (0.14 nm⁻²) and Mo SAs/ML-MoS₂ (0.24 nm⁻²) samples, which are quite low and close to each other.^{26,35,42} Meanwhile, Mo vacancies were seldomly found in the Mo SAs/ML-MoS₂ sample which indicates that the Mo SAs may originate from the edges of the MoS₂ flakes, due to their lower cohesive energy than those in the basal plane. Similarly, a considerable amount of W SAs (1.76×10^{13} atoms cm⁻²) were synthesized on monolayer WS₂ after the same plasma treatment (**Figure 1E**). Taken together, these results demonstrate that the metal SAs/2D monolayer systems with a high loading of different metal SAs were synthesized after the cold hydrogen plasma reduction of different 2D monolayers.

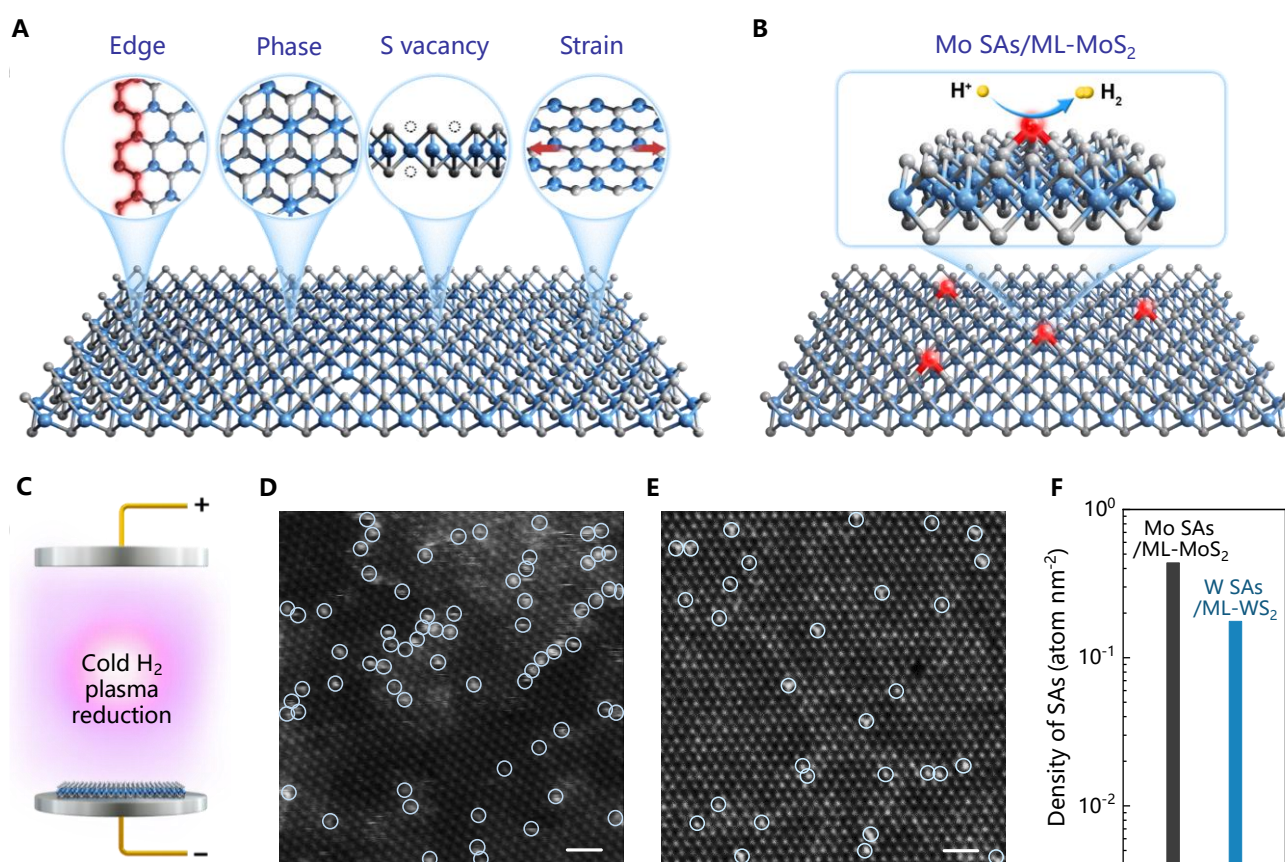


Figure 1. Formation of metal SAs on 2D monolayers. (A) Schematic showing representative active

sites of MoS₂ for hydrogen evolution reported previously, including edges, S vacancies, 1T phase, and strain. (B) Schematic showing Mo SAs/ML-MoS₂ as a new active site for hydrogen evolution. (C) Schematic showing the synthesis of metal SAs on cogenetic 2D monolayer by cold hydrogen plasma reduction. (D,E) HAADF-STEM images of (D) Mo SAs/ML-MoS₂ and (E) W SAs/ML-WS₂ samples, showing high densities of Mo and W SAs in the samples. The scale bar is 1 nm for d and e. (F) Statistical results of the density of Mo and W SAs on 2D monolayers.

To further confirm that the bright spots are Mo single atoms on ML-MoS₂ and to study their local configuration, we carried out detailed HAADF-STEM analyses. The full width at half maximum (FWHM) of the intensity profile of each brighter site was collected from the HAADF-STEM images, and statistical analysis showed a narrow size distribution with an average size of 0.16 nm for single atoms resolved in 60 kV STEM images (**Figure 2A**). This average size is slightly larger than that of Mo (IV) atoms (0.14 nm) in the MoS₂ basal plane, which may be attributed to the larger Debye–Waller factor of a Mo SA due to its unsaturated bonding. Intensity profile analysis of an enlarged HAADF-STEM image revealed (**Figure 2B**) that the brighter sites (blue spot marked with 2) have nearly double the intensity of the Mo sites in the basal plane of MoS₂ (blue spot marked with 1), suggesting a Mo SA sitting on top of a Mo atom of MoS₂ (**Figure 2B**). Moreover, the corresponding fast Fourier transform (FFT) pattern (**Figure 2C**) shows no obvious changes of the lattice parameters along the [0001] zone axis, suggesting that the Mo SAs have a negligible effect on the lattice structure of underlying monolayer MoS₂. Careful examination on tens of Mo SAs showed that the Mo SAs/ML-MoS₂ catalyst contained two types of Mo SAs, one sitting on Mo atop sites (Mo SA-1 in **Figure 2D**) and the other sitting above S vacancy sites (Mo SA-2 in **Figure S12**) in the MoS₂ basal plane. Statistical

analysis shows that around two thirds of the Mo SAs are type 1 and one third are type 2. The structures of these two types were studied by density functional theory (DFT) calculations to understand their coordination status, and their relaxation structures and a comparison with experimental results are shown in **Figure S13**. As discussed later, both configurations were found to be active in the HER reaction. Similarly, we also carried out detailed HAADF-STEM analyses and simulations on the W SAs/ML-WS₂ samples, showing that W SAs are sitting either on the atop site of W atoms in the WS₂ or above S vacancy sites (**Figures S14 and S15**).

Taking Mo SAs/ML-MoS₂ system as an example, we studied the samples and found that unlike saturated Mo atoms in MoS₂ basal plane where each Mo atom bond with six sulfur atoms, the Mo SAs on the basal plane of MoS₂ are unsaturated. To study their chemical environment in the Mo SAs/ML-MoS₂ sample, we carried out high resolution XPS measurements. **Figure 2E** shows that the Mo 3*d* peak of the Mo SAs/ML-MoS₂ sample shifts greatly to a lower binding energy than that of the pristine MoS₂ sample. For example, a large binding energy shift of the Mo 3*d*_{2/5} peak (-0.57 eV) is observed for a sample after hydrogen plasma treatment for 80 s (**Figure S16**). In addition, the Mo 3*d*_{2/5} and Mo 3*d*_{2/3} peaks show a larger FWHM because of the existence of both Mo (IV) in the MoS₂ basal planes and Mo SAs on the surface with a smaller binding energy (**Figure 2E**). Each Mo (IV) atom in the basal plane is bonded to six S atoms, while a Mo SA only bond to three S atoms or bond to two S atoms and leaves a S vacancy. As a result, the S/Mo ratio decreases with increasing plasma treatment time, as revealed by both XPS and STEM results (**Figure S17**). To summary the unsaturated coordination of Mo single atoms on monolayer MoS₂, **Figure 2F** shows the ratio of the number of unsaturated Mo atoms in the Mo SAs/ML-MoS₂ and pristine MoS₂ samples to the total number of Mo atoms, where

unsaturated Mo atoms are defined as those that are not bonded to six S atoms (*i.e.*, Mo SAs and Mo atoms in the basal plane of MoS₂ adjacent to S vacancy). Moreover, the calculated Bader charges (**Figure 2G**) show that the all Mo atoms are positively charged. A Mo atom in pristine MoS₂ loses 1.06 *e*, which is more than the 0.83 *e* for Mo SA-1 and 0.58 *e* for Mo SA-2. Therefore, Mo SAs transfer less charge to sulfur atoms than do saturated Mo atoms in pristine MoS₂, showing that the Mo SAs are unsaturated. Both experiment and theoretical calculations give consistent results, that is, unsaturated Mo SAs are formed on the MoS₂ in Mo SAs/ML-MoS₂ samples.

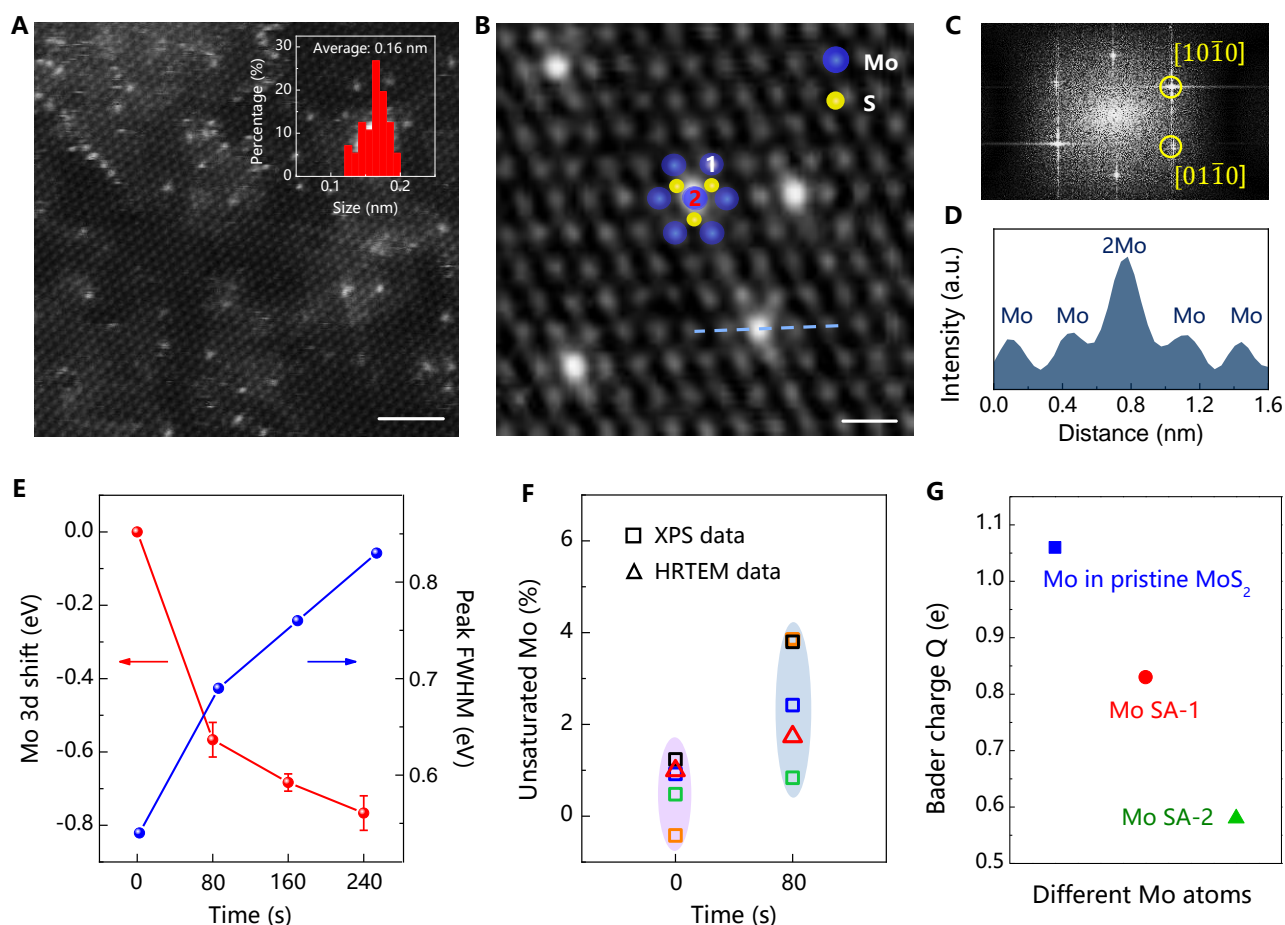


Figure 2. Structural and chemical characterization of the Mo SAs/ML-MoS₂ samples. (A) HAADF-STEM image and size distribution of the Mo SAs. (B) Enlarged HAADF-STEM image, (C) corresponding FFT pattern, and (D) intensity profile along the blue line in B. The results indicate that

Mo SAs sitting on top of Mo atoms in the MoS₂ basal planes. (E) Statistical results of the positions and FWHM of the Mo 3d_{3/2} XPS peak for MoS₂ samples treated in hydrogen plasma for different time. Data were measured three times for each sample, and error bars correspond to the standard deviations. (F) XPS and HRTEM results showing the ratio of unsaturated Mo to all Mo atoms for Mo SAs/ML-MoS₂ samples. The XPS data was collected from four different samples for both pristine MoS₂ and Mo SAs/ML-MoS₂. (G) Bader charges of Mo atoms in different configurations, including Mo in the pristine MoS₂ (blue square), Mo SA sitting on the Mo atop sites of MoS₂ basal plane (*i.e.*, Mo SA-1, red circle), and Mo SA sitting above the S vacancy sites (*i.e.*, Mo SA-2, green triangle). The scale bars are 2 nm for a and 0.5 nm for B.

We then tested the HER performance of a Mo SAs/ML-MoS₂ catalyst which lay on a SiO₂/Si substrate. Unlike conventional powder catalysts, the key feature of the Mo SAs/ML-MoS₂ catalyst is that we can accurately determine the areas and numbers of active sites by using a microreactor design (**Figure 3A**). A typical two-terminal device was fabricated using e-beam lithography, where a pristine ML-MoS₂ flake were covered by polymethyl methacrylate (PMMA) with exposure of certain areas of the basal plane and two electrode pads (see device fabrication details in Methods and **Figure S18**).¹⁵⁻
¹⁷ The PMMA layer not only protects the device from acidic or alkaline electrolytes (**Figures S19 and S20**), but it also ensures that only the pre-defined exposed area of catalyst is in contact with the electrolyte. After the hydrogen plasma treatment, only the exposed MoS₂ area has been converted into Mo SAs/ML-MoS₂ (**Figure 3B and Figure S21**). A microreactor was used for electrocatalytic HER measurements of the MoS₂ flake exposed to both acidic (0.5 M H₂SO₄) and alkaline (1.0 M KOH) medium (**Figures 3C and 3D**). Notably, in this experiment, Mo SA/ML-MoS₂ came from the pristine

MoS₂ sample, which ensures the same surface area and device design. Therefore, we were able to directly study how the new Mo SA sites in Mo SAs/ML-MoS₂ contributed to the HER.

We first tested Pt-based electrocatalysts in the same microreactor design, which showed comparable results to a normal electrochemical reactor, suggesting the good reliability of the microreactor (**Figure S19**). For MoS₂-based catalysts, the polarization curves of the pristine MoS₂ and Mo SAs/ML-MoS₂ samples in both H₂SO₄ and KOH solutions are shown in **Figure 3E**. The catalytic performance of the pristine MoS₂ was comparable to that of monolayer MoS₂ catalysts recently reported (**Table S1**). Impressively, we found that the Mo SAs/ML-MoS₂ sample requires much smaller overpotentials to reach the same current densities than the pristine MoS₂. For example, the basal plane of Mo SAs/ML-MoS₂ shows remarkable HER performance in acidic medium, with an overpotential of 107 mV (versus RHE) at a current density of 10 mA cm⁻² and an overpotential of 261 mV (versus RHE) at a current density of 400 mA cm⁻², which are among the best values in 2D MoS₂-based electrocatalysts (**Table S1**). At overpotentials of 150 mV or 200 mV, the current densities of the Mo SAs/ML-MoS₂ are 30-times or 180-times higher than that of the pristine MoS₂, respectively. In alkaline medium, the Mo SAs/ML-MoS₂ sample also showed decent HER performance with an overpotential of 209 mV at a current density of 10 mA cm⁻², which is smaller than the pristine MoS₂ sample (322 mV at 10 mA cm⁻²). We note that MoS₂ electrocatalysts show a slower charge transfer process in alkaline than in acidic medium, presumably related to sluggish water dissociation on the MoS₂ surface in alkaline medium, as previously reported.^{9,43,44} The overpotentials required to achieve a current density of 10 mA cm⁻² for different samples are summarized in **Figure S22A**. The device remains good after all the tests, suggesting that only the exposed basal plane of MoS₂ was involved in the electrochemical process (**Figure S23**).

The model electrocatalysts using the ML-MoS₂ on the substrate provide unique platforms for studying the HER kinetics of Mo SA sites. It is known that the kinetics analyses of heterogeneous reactions require an accurate interfacial area, however this is challenging to quantify in practical situations. For conventional electrochemical cells, catalysts are loaded on conductive substrates in powder or film forms, resulting in a ratio of interfacial surface area to surface area of electrode ($A_{\text{int}}/A_{\text{ele}}$) that is larger than one, but difficult to determine accurately. Direct use of geometrical surface area will overestimate the activity of a catalyst.⁴⁵ Other methods such as electrochemical surface area (ECSA) measurements have limitations for complex catalysts and can be affected by testing conditions. Here, we combined the microreactor design and monolayer nature of the MoS₂ on a substrate with encapsulation to make $A_{\text{interface}}/A_{\text{electrode}}$ close to one, making it feasible to quantitatively study the HER kinetics of Mo SAs/ML-MoS₂ (**Figure S1**). To analyze the rate-determining steps of catalysts, the Butler-Volmer equation and its derivations are usually used. Using the Tafel plots of the two samples, the Tafel slopes were obtained from the linear region (**Figure 3F**). The pristine MoS₂ sample shows Tafel slopes of 79.2 mV dec⁻¹ in acid and 108.4 mV dec⁻¹ in alkali, similar to other reports.^{15,33,35} Based on previous studies,^{8,9,34,46} the rate-determining step for the pristine MoS₂ catalysts should be the Volmer step,⁹ a step of the primary discharge of protons. In sharp contrast, the Mo SAs/ML-MoS₂ catalyst shows very small Tafel slopes of 35.1 mV dec⁻¹ in acid and 36.4 mV dec⁻¹ in alkali, close to the theoretical value of 40 mV dec⁻¹ at which the Heyrovsky reaction pathway is the rate-determining step. The lower Tafel slope of Mo SAs/ML-MoS₂ than pristine MoS₂ indicates fast HER kinetics for the Mo SAs/ML-MoS₂. Tafel slopes for different samples are summarized in **Figure S22B**. The fast HER kinetics of the Mo SAs/ML-MoS₂ is further confirmed by the TOF analyses (**Note S1 and Figure S22C**). For example, the TOF of the Mo SAs/ML-MoS₂ catalyst is as high as $\sim 10^3$ s⁻¹ at 100 mV. In

addition, the samples do not show obvious changes after repeated tests (**Figure S24**). These results indicate that Mo SAs/ML-MoS₂ is a new type of active site for MoS₂ that shows fast HER kinetics.

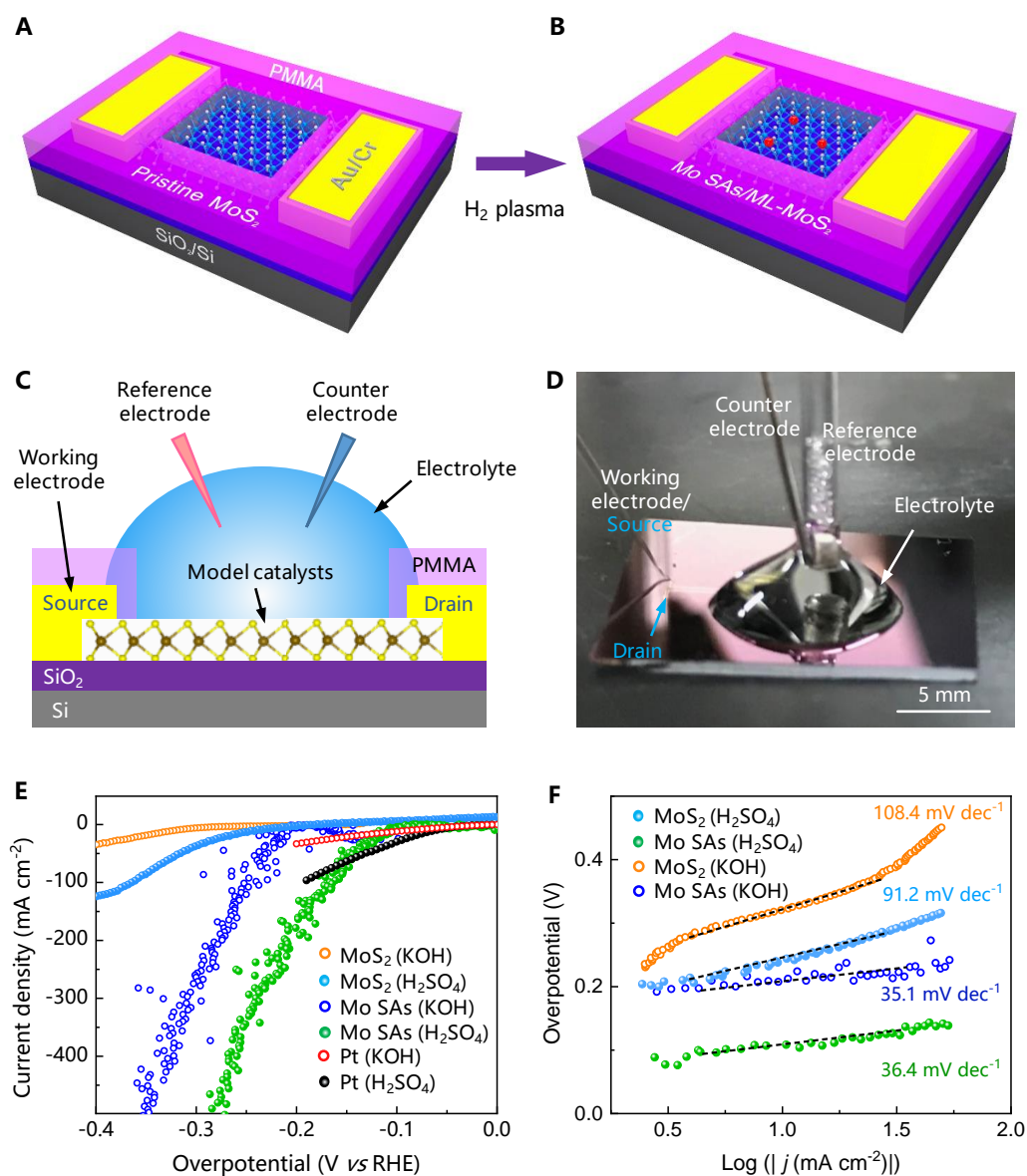


Figure 3. Electrochemical performance of the Mo SAs/ML-MoS₂ catalysts. (A,B) Schematics showing a ML-MoS₂ flake (A) before and (B) after hydrogen plasma treatment, where only a certain area of the MoS₂ was exposed for hydrogen plasma treatment and subsequent electrochemical tests. (C) Schematic and (D) optical image showing the electrochemical microreactor based on a ML-MoS₂ flake. (E) Polarization curves and (F) Tafel plots of the pristine ML-MoS₂, Mo SAs/ML-MoS₂, and Pt

samples in H₂SO₄ (0.5 M) and KOH (1.0 M). Interfacial surface areas used for calculation of current densities were obtained from the exposed surface area of each device, which was accurately determined during the electron beam lithography process.

DISCUSSION

We carried out DFT calculations to elucidate the effects of unsaturated Mo SAs on the catalytic activity of Mo SAs/ML-MoS₂. Mo atoms in intact MoS₂ monolayer were also included for a better understanding of this issue. The relaxed structures of the pristine MoS₂, Mo SA-1, S vacancy, and Mo SA-2 are shown in **Figures 4A-D**. Here, the calculated Gibbs free energies of hydrogen adsorption (ΔG_{H}) on these structures are shown in **Figure 4E**, with their optimized configurations shown in **Figure S25**. It is generally accepted that an almost zero ΔG_{H} shows a good HER electrocatalyst.⁴⁷ A large positive/negative ΔG_{H} suggests the existence of a large energy barrier in the processes of hydrogen adsorption/desorption. We found that hydrogen is difficult to adsorb on Mo sites in a pristine MoS₂ basal plane with a large ΔG_{H} of 2.356 eV, leading to sluggish HER kinetics (**Figure 4E**). In contrast, Mo SAs on MoS₂ are found to be efficient sites for HER, because hydrogen can easily adsorb and desorb with small hydrogen free energy of 0.003 eV (Mo SA-1 site) and -0.114 eV (at Mo SA-2 site), which are comparable with or even smaller than 0.041 eV for MoS₂ with a S vacancy, a well-recognized HER active site.²⁵ These results suggest that isolated Mo SAs on a MoS₂ surface, especially the Mo SA-1, is a new active center for ultrafast hydrogen evolution.

To further understand the improved catalytic activity of Mo SAs/ML-MoS₂ compared to the pristine MoS₂, we analyzed the projected density of states (PDOS) of adsorbed hydrogen atoms on the different structures shown in **Figures 4A-D**. For the pristine MoS₂, the PDOS of H shows well-isolated

sharp peaks below the Fermi level, indicating weak bonding behavior of H. Accordingly, the Fermi level is pinned at the conduction band minimum of MoS₂, which is consistent with an earlier report that considered the lowest unoccupied state as the indicator for the bonding strength of H.⁴⁸ In contrast, for the other three cases, there are clear hybridized bonding and anti-bonding states below and above the Fermi level with wider peaks. These different bonding characterizations are easily seen from the typical partial charge density distributions (insets of **Figure 4F**), for the hybridized bonding states of a hydrogen atom adsorbed in the different cases. Hybridization between H and Mo orbitals not only increases chemical bonding but lowers the Fermi level compared to the pristine case (indicated by vertical arrows in **Figure 4F**), both of which lead to a lower ΔG_H .

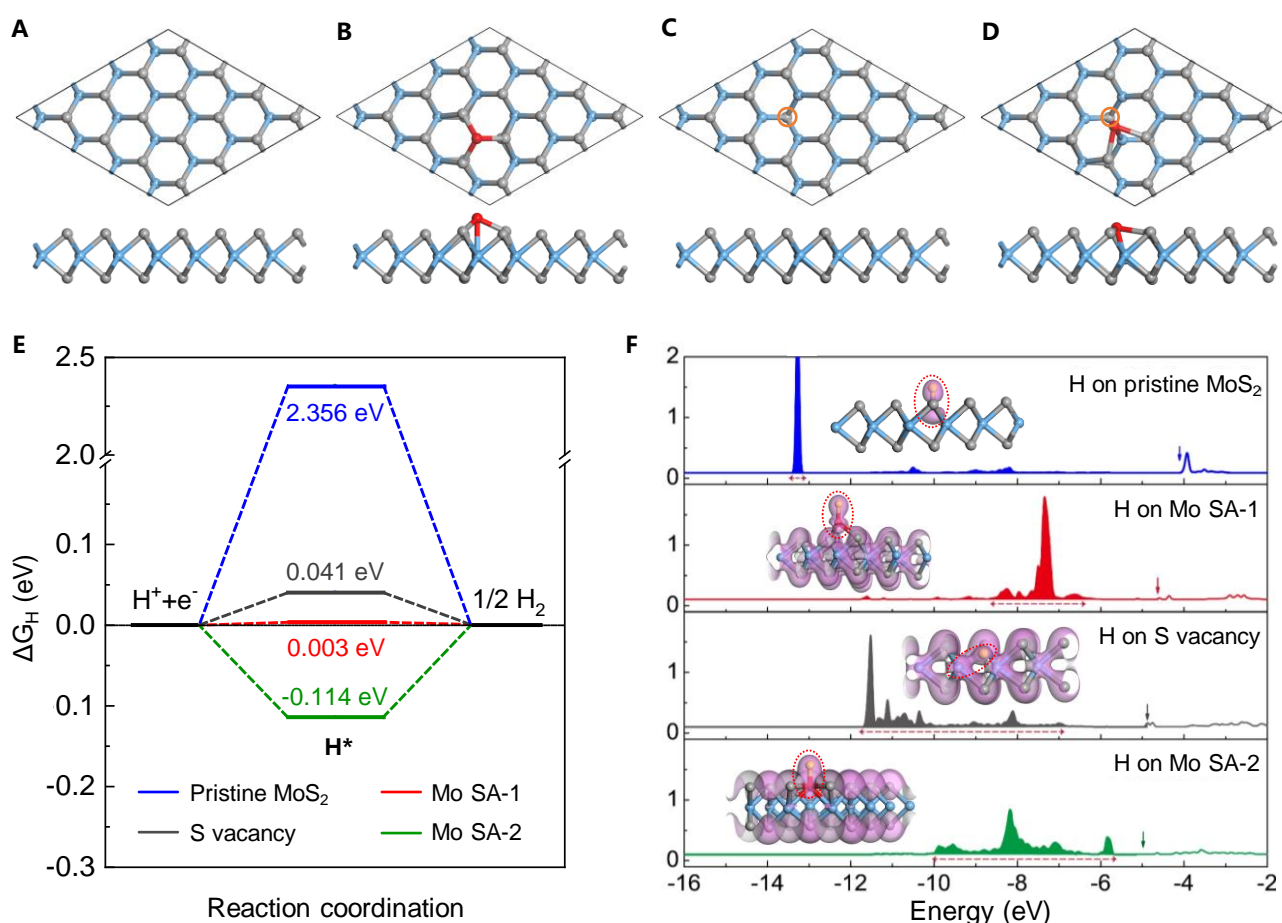


Figure 4. Theoretical analyses. (A-D) Top view and side view of the slab models used to describe the

(A) pristine MoS₂, (B) Mo SA-1, (C) S vacancy, and (D) Mo SA-2. Atoms in grey and blue represent the S and Mo atoms of the MoS₂, Mo SAs are highlighted in red, and S vacancies are highlighted by orange circles. e Free energy profiles of HER at the equilibrium potential for Mo atoms at the basal plane of the pristine MoS₂ (blue line), S vacancy (grey line), Mo SA-1 (red line), and Mo SA-2 (green line). Compared to saturated Mo atoms in the basal plane, S vacancies and Mo SA/ML-MoS₂ are unsaturated and show fast HER kinetics theoretically. (F) PDOS of adsorbed hydrogen atoms for different MoS₂ configurations, *i.e.*, pristine (blue line), S vacancy (grey line), Mo SA-1 (red line) and Mo SA-2 (green line). The occupied states are filled with different colors, and unoccupied states are unfilled. The vertical arrows indicate the Fermi level. The energy levels are referenced to the vacuum level. The insets from top to bottom in panel F are the partial charge density distribution for characteristic bonding states in the energy range that indicated by horizontal dashed arrows for different cases. The isovalues of charge density are 0.1 e/Å³ for pristine MoS₂ and the Mo SA-1 cases and 0.25 e/Å³ for the S vacancy and Mo SA-2 cases to clearly display the bonding states between hydrogen atoms and substrates, which are highlighted by red dotted ellipses.

In conclusion, we developed a cold hydrogen plasma reduction method and synthesized different metal single atoms on 2D monolayer systems. We further fabricated a 2D model electrocatalyst made of Mo single atoms on a cogenetic monolayer MoS₂, which shows a superior improvement of the HER activity compared to pristine MoS₂. Experimental and theoretical results indicate that Mo single atoms on monolayer MoS₂ are a new type of active site for HER with ultrafast hydrogen adsorption/desorption kinetics, originating from a strong hybridization between the single Mo atoms and hydrogen atoms. This work opens an alternative strategy to design high performance MoS₂-based

catalysts to generate hydrogen by electrochemical water splitting. The cold plasma reduction method addressed the current challenge of synthesizing high loading amounts of single atoms on 2D monolayers. In addition, other metal single atoms could in principle be synthesized from their corresponding transition metal chalcogenides to make a family of metal single atoms/2D monolayers, since they show similar formation free energies of their metal atoms with MoS₂ and WS₂.⁴⁰ The formation of single atoms on monolayer 2D materials with clear and well-defined structures offers valuable platforms to study various electrochemical processes beyond hydrogen evolution discussed here, including lithium-sulphur batteries, fuel cells, and photoelectrochemical devices.

EXPERIMENTAL PROCEDURES

Full details of experimental procedures are provided in the Supplemental Information.

SUPPLEMENTAL INFORMATION

Supplemental Information includes Supplemental Experimental Procedures, 25 figures, and 3 tables and 1 note can be found with this article online.

AUTHOR CONTRIBUTIONS

Y.L. and B.L. conceived the idea and directed the research. M.L., Q.F., and Z.C. synthesized MoS₂ flakes by CVD method. L.T. synthesized WS₂ flakes by CVD method. Y.L. and S.X. performed the plasma treatment experiments under guidance of W. L.. Y.L. and L.T. performed Raman, SEM, XPS, and AFM characterization. H.P. and Y.L. fabricated microcell devices under guidance of Y.Z.. B.D. and U.K. helped in electronic device measurements. Y.L. performed the electrochemical tests with help from B.D.. Z.G. and J.L. performed TEM experiments. S.Z. and X.Z. performed the theoretical calculations. Y.L, S.Z., J.L., X.Z., H.M.C., and B.L. analyzed the data, interpreted the results and wrote

the manuscript with feedbacks from the other authors.

ACKNOWLEDGMENTS

We sincerely thank Prof. Andre Geim for fruitful discussions and inputs to this work. We also thank Prof. Hengqiang Ye for the analyses of TEM data, and Chi Zhang, Zhiyuan Zhang, and Dr. Qiangmin Yu for help in the electrochemical measurements. We acknowledge support by the National Natural Science Foundation of China (Nos. 51722206 and 11674150), the Youth 1000-Talent Program of China, Guangdong Innovative and Entrepreneurial Research Team Program (Nos. 2017ZT07C341 and 2016ZT06D348), the Economic, Trade and Information Commission of Shenzhen Municipality for the “2017 Graphene Manufacturing Innovation Center Project” (No. 201901171523), Shenzhen Science and Technology Innovation Commission (JCYJ20160613160524999) and the Development and Reform Commission of Shenzhen Municipality for the development of the “Low-Dimensional Materials and Devices” discipline.

REFERENCES

- 1 Deng, D., Novoselov, K. S., Fu, Q., Zheng, N., Tian, Z., and Bao, X. (2016). Catalysis with two-dimensional materials and their heterostructures. *Nat. Nanotechnol.* *11*, 218-230.
- 2 Seh, Z. W., Kibsgaard, J., Dickens, C. F., Chorkendorff, I., Norskov, J. K., and Jaramillo, T. F. (2017). Combining theory and experiment in electrocatalysis: Insights into materials design. *Science* *355*, 1-12.
- 3 Staszak-Jirkovsky, J., Malliakas, C. D., Lopes, P. P., Danilovic, N., Kota, S. S., Chang, K.-C., Genorio, B., Strmcnik, D., Stamenkovic, V. R., Kanatzidis, M. G., and Markovic, N. M. (2016). Design of active and stable Co-Mo-S_x chalcogels as pH-universal catalysts for the hydrogen evolution reaction. *Nat. Mater.* *15*, 197-203.
- 4 Chen, Y.-Y., Zhang, Y., Zhang, X., Tang, T., Luo, H., Niu, S., Dai, Z.-H., Wan, L.-J., and Hu, J.-S. (2017). Self-templated fabrication of MoNi₄/MoO_{3-x} nanorod arrays with dual active components for highly efficient hydrogen evolution. *Adv. Mater.* *29*, 1703311.
- 5 Liang, J., Ma, F., Hwang, S., Wang, X., Sokolowski, J., Li, Q., Wu, G., and Su, D. (2019).

Atomic Arrangement Engineering of Metallic Nanocrystals for Energy-Conversion Electrocatalysis. *Joule* 3, 956-991.

- 6 Subbaraman, R., Tripkovic, D., Strmcnik, D., Chang, K.-C., Uchimura, M., Paulikas, A. P., Stamenkovic, V., and Markovic, N. M. (2011). Enhancing hydrogen evolution activity in water splitting by tailoring Li^+ - $\text{Ni}(\text{OH})_2$ -Pt interfaces. *Science* 334, 1256-1260.
- 7 Danilovic, N., Subbaraman, R., Strmcnik, D., Chang, K. C., Paulikas, A. P., Stamenkovic, V. R., and Markovic, N. M. (2012). Enhancing the alkaline hydrogen evolution reaction activity through the bifunctionality of $\text{Ni}(\text{OH})_2$ /metal catalysts. *Angew. Chem. Int. Ed.* 51, 12495-12498.
- 8 Li, G., Zhang, D., Yu, Y., Huang, S., Yang, W., and Cao, L. (2017). Activating MoS_2 for pH-universal hydrogen evolution catalysis. *J. Am. Chem. Soc.* 139, 16194-16200.
- 9 Luo, Y., Li, X., Cai, X., Zou, X., Kang, F., Cheng, H. M., and Liu, B. (2018). Two-dimensional MoS_2 confined $\text{Co}(\text{OH})_2$ electrocatalysts for hydrogen evolution in alkaline electrolytes. *ACS Nano* 12, 4565-4573.
- 10 Hu, J., Zhang, C., Jiang, L., Lin, H., An, Y., Zhou, D., Leung, M. K. H., and Yang, S. (2017). Nanohybridization of MoS_2 with Layered Double Hydroxides Efficiently Synergizes the Hydrogen Evolution in Alkaline Media. *Joule* 1, 383-393.
- 11 Shi, Z., Nie, K., Shao, Z.-J., Gao, B., Lin, H., Zhang, H., Liu, B., Wang, Y., Zhang, Y., Sun, X., Cao, X.-M., Hu, P., Gao, Q., and Tang, Y. (2017). Phosphorus- Mo_2C @carbon nanowires toward efficient electrochemical hydrogen evolution: composition, structural and electronic regulation. *Energy Environ. Sci.* 10, 1262-1271.
- 12 Han, N., Yang, K. R., Lu, Z., Li, Y., Xu, W., Gao, T., Cai, Z., Zhang, Y., Batista, V. S., Liu, W., and Sun, X. (2018). Nitrogen-doped tungsten carbide nanoarray as an efficient bifunctional electrocatalyst for water splitting in acid. *Nat. Commun.* 9, 924.
- 13 Zhang, G., Wang, G., Liu, Y., Liu, H., Qu, J., and Li, J. (2016). Highly active and stable catalysts of phytic acid-derivative transition metal phosphides for full water splitting. *J. Am. Chem. Soc.* 138, 14686-14693.
- 14 Li, J., Li, J., Zhou, X., Xia, Z., Gao, W., Ma, Y., and Qu, Y. (2016). Highly efficient and robust nickel phosphides as bifunctional electrocatalysts for overall water-splitting. *ACS Appl. Mater.*

Interfaces 8, 10826-10834.

- 15 Voiry, D., Fullon, R., Yang, J., de Carvalho Castro, E. S. C., Kappera, R., Bozkurt, I., Kaplan, D., Lagos, M. J., Batson, P. E., Gupta, G., Mohite, A. D., Dong, L., Er, D., Shenoy, V. B., Asefa, T., and Chhowalla, M. (2016). The role of electronic coupling between substrate and 2D MoS₂ nanosheets in electrocatalytic production of hydrogen. *Nat. Mater.* 15, 1003-1009.
- 16 Wang, J., Yan, M., Zhao, K., Liao, X., Wang, P., Pan, X., Yang, W., and Mai, L. (2017). Field effect enhanced hydrogen evolution reaction of MoS₂ nanosheets. *Adv. Mater.* 29, 1604464.
- 17 Zhang, J., Wu, J., Zou, X., Hackenberg, K., Zhou, W., Chen, W., Yuan, J., Keyshar, K., Gupta, G., Mohite, A., Ajayan, P. M., and Lou, J. (2019). Discovering superior basal plane active two-dimensional catalysts for hydrogen evolution. *Mater. Today* 25, 28-34.
- 18 Cai, X., Luo, Y., Liu, B., and Cheng, H.-M. (2018). Preparation of 2D material dispersions and their applications. *Chem. Soc. Rev.* 47, 6224-6266.
- 19 Tributsch, H., and Bennett, J. C. (1977). Electrochemistry and photochemistry of MoS₂ layer crystals. *J. Electroanal. Chem.* 81, 97-111.
- 20 Grange, P. (2006). Catalytic hydrodesulfurization. *Catal. Rev.* 21, 135-181.
- 21 Thomas F. Jaramillo, Kristina P. Jørgensen, Jacob Bonde, Jane H. Nielsen, Sebastian Horch, and Chorkendorff, I. (2007). Identification of active edge sites for electrochemical H₂ evolution from MoS₂ nanocatalysts. *Science* 317, 100-102.
- 22 Hinnemann, B., Moses, P. G., Bonde, J., Jørgensen, K. P., Nielsen, J. H., Horch, S., Chorkendorff, I., and Nørskov, J. K. (2005). Biomimetic hydrogen evolution: MoS₂ nanoparticles on graphite as catalyst for hydrogen evolution. *J. Am. Chem. Soc.* 127, 5308-5309.
- 23 Lukowski, M. A., Daniel, A. S., Meng, F., Forticaux, A., Li, L., and Jin, S. (2013). Enhanced hydrogen evolution catalysis from chemically exfoliated metallic MoS₂ nanosheets. *J. Am. Chem. Soc.* 135, 10274-10277.
- 24 Chhowalla, M., Shin, H. S., Eda, G., Li, L.-J., Loh, K. P., and Zhang, H. (2013). The chemistry of two-dimensional layered transition metal dichalcogenide nanosheets. *Nat. Chem.* 5, 263-275.
- 25 Tsai, C., Li, H., Park, S., Park, J., Han, H. S., Nørskov, J. K., Zheng, X., and Abild-Pedersen,

- F. (2017). Electrochemical generation of sulfur vacancies in the basal plane of MoS₂ for hydrogen evolution. *Nat. Commun.* *8*, 15113.
- 26 Li, H., Tsai, C., Koh, A. L., Cai, L., Contryman, A. W., Fragapane, A. H., Zhao, J., Han, H. S., Manoharan, H. C., Abild-Pedersen, F., Norskov, J. K., and Zheng, X. (2016). Activating and optimizing MoS₂ basal planes for hydrogen evolution through the formation of strained sulphur vacancies. *Nat. Mater.* *15*, 364.
- 27 Xie, J., Zhang, J., Li, S., Grote, F., Zhang, X., Zhang, H., Wang, R., Lei, Y., Pan, B., and Xie, Y. (2013). Controllable disorder engineering in oxygen-incorporated MoS₂ ultrathin nanosheets for efficient hydrogen evolution. *J. Am. Chem. Soc.* *135*, 17881-17888.
- 28 Geng, X., Sun, W., Wu, W., Chen, B., Al-Hilo, A., Benamara, M., Zhu, H., Watanabe, F., Cui, J., and Chen, T. P. (2016). Pure and stable metallic phase molybdenum disulfide nanosheets for hydrogen evolution reaction. *Nat. Commun.* *7*, 10672.
- 29 Tang, C., Zhong, L., Zhang, B., Wang, H. F., and Zhang, Q. (2018). 3D mesoporous van der Waals heterostructures for trifunctional energy electrocatalysis. *Adv. Mater.* *30*, 1705110.
- 30 Yu, Y., Nam, G.-H., He, Q., Wu, X.-J., Zhang, K., Yang, Z., Chen, J., Ma, Q., Zhao, M., Liu, Z., Ran, F.-R., Wang, X., Huang, X., Li, B., Xiong, Q., Zhang, Q., Liu, Z., Gu, L., Huang, W., Du, Y., and Zhang, H. (2018). High phase-purity 1T'-MoS₂ and 1T'-MoSe₂-layered crystals. *Nat. Chem.* *10*, 638–643.
- 31 Luo, Z., Ouyang, Y., Zhang, H., Xiao, M., Ge, J., Jiang, Z., Wang, J., Tang, D., Cao, X., Liu, C., and Xing, W. (2018). Chemically activating MoS₂ via spontaneous atomic palladium interfacial doping towards efficient hydrogen evolution. *Nat. Commun.* *9*, 2120.
- 32 Zhou, Y., Silva, J. L., Woods, J. M., Pondick, J. V., Feng, Q., Liang, Z., Liu, W., Lin, L., Deng, B., Brena, B., Xia, F., Peng, H., Liu, Z., Wang, H., Araujo, C. M., and Cha, J. J. (2018). Revealing the contribution of individual factors to hydrogen evolution reaction catalytic activity. *Adv. Mater.*, 1706076.
- 33 Zhang, J., Wu, J., Guo, H., Chen, W., Yuan, J., Martinez, U., Gupta, G., Mohite, A., Ajayan, P. M., and Lou, J. (2017). Unveiling active sites for the hydrogen evolution reaction on monolayer MoS₂. *Adv. Mater.* *29*, 1701955.
- 34 Jaramillo, T. F., Jørgensen, K. P., Bonde, J., Nielsen, J. H., Horch, S., and Chorkendorff, I.

- (2007). Identification of active edge sites for electrochemical H₂ evolution from MoS₂ nanocatalysts. *Science* *6*, 100-102.
- 35 Yu, Y., Huang, S.-Y., Li, Y., Steinmann, S. N., Yang, W., and Cao, L. (2014). Layer-dependent electrocatalysis of MoS₂ for hydrogen evolution. *Nano Lett.* *14*, 553-558.
- 36 Chen, Y., Ji, S., Chen, C., Peng, Q., Wang, D., and Li, Y. (2018). Single-Atom Catalysts: Synthetic Strategies and Electrochemical Applications. *Joule* *2*, 1242-1264.
- 37 Guan, J., Duan, Z., Zhang, F., Kelly, S. D., Si, R., Dupuis, M., Huang, Q., Chen, J. Q., Tang, C., and Li, C. (2018). Water oxidation on a mononuclear manganese heterogeneous catalyst. *Nat. Catal.* *1*, 870-877.
- 38 Sabat, K. C., Paramguru, R. K., Pradhan, S., and Mishra, B. K. (2015). Reduction of cobalt oxide (Co₃O₄) by low temperature hydrogen plasma. *Plasma Chem. Plasma Process.* *35*, 387–399.
- 39 Sabat, K. C., Rajput, P., Paramguru, R. K., and Mishra, B. B. B. K. (2014). Reduction of oxide minerals by hydrogen plasma: an overview. *Plasma Chem. Plasma Process.* *34*, 1-23.
- 40 Reed, T. B. *Free energy of formation of binary compounds: an atlas of charts for high-temperature chemical calculations.* (Mass: MIT Press, 1971).
- 41 Kiriya, D., Lobaccaro, P., Nyein, H. Y., Taheri, P., Hettick, M., Shiraki, H., Sutter-Fella, C. M., Zhao, P., Gao, W., Maboudian, R., Ager, J. W., and Javey, A. (2016). General thermal texturization process of MoS₂ for efficient electrocatalytic hydrogen evolution reaction. *Nano Lett.* *16*, 4047-4053.
- 42 Hong, J., Hu, Z., Probert, M., Li, K., Lv, D., Yang, X., Gu, L., Mao, N., Feng, Q., Xie, L., Zhang, J., Wu, D., Zhang, Z., Jin, C., Ji, W., Zhang, X., Yuan, J., and Zhang, Z. (2015). Exploring atomic defects in molybdenum disulphide monolayers. *Nat. Commun.* *6*, 6293.
- 43 Zhang, J., Wang, T., Liu, P., Liu, S., Dong, R., Zhuang, X., Chen, M., and Feng, X. (2016). Engineering water dissociation sites in MoS₂ nanosheets for accelerated electrocatalytic hydrogen production. *Energy Environ. Sci.* *9*, 2789-2793.
- 44 Luo, Y., Tang, L., Khan, U., Yu, Q., Cheng, H.-M., Zou, X., and Liu, B. (2019). Morphology and surface chemistry engineering toward pH-universal catalysts for hydrogen evolution at high current density. *Nat. Commun.* *10*, 269.

- 45 Sun, S., Li, H., and Xu, Z. J. (2018). Impact of surface area in evaluation of catalyst activity. *Joule* 2, 1024-1027.
- 46 Voiry, D., Yamaguchi, H., Li, J., Silva, R., Alves, D. C., Fujita, T., Chen, M., Asefa, T., Shenoy, V. B., Eda, G., and Chhowalla, M. (2013). Enhanced catalytic activity in strained chemically exfoliated WS₂ nanosheets for hydrogen evolution. *Nat. Mater.* 12, 850-855.
- 47 Greeley, J., Jaramillo, T. F., Bonde, J., Chorkendorff, I. B., and Norskov, J. K. (2006). Computational high-throughput screening of electrocatalytic materials for hydrogen evolution. *Nat. Mater.* 5, 909-913.
- 48 Liu, Y., Wu, J., Hackenberg, K. P., Zhang, J., Wang, Y. M., Yang, Y., Keyshar, K., Gu, J., Ogitsu, T., Vajtai, R., Lou, J., Ajayan, P. M., Wood, Brandon C., and Yakobson, B. I. (2017). Self-optimizing, highly surface-active layered metal dichalcogenide catalysts for hydrogen evolution. *Nat. Energy* 2, 17127.